J Mater Sci (2016) 51:6913–6932

Continuous carbon fiber polymer–matrix composites in unprecedented antiferroelectric coupling providing exceptionally high through-thickness electric permittivity

Yoshihiro Takizawa[1] and D. D. L. Chung[1,*]

[1] *Composite Materials Research Laboratory, University at Buffalo, State University of New York Buffalo, Buffalo, NY 14260-4400, USA*

Received: 25 February 2016
Accepted: 11 April 2016
Published online: 25 April 2016

ABSTRACT

Continuous carbon fiber polymer–matrix composites in unprecedented antiferroelectric coupling, as enabled by stacking composites with positive value (up to 400) and negative value (down to −600) of the electric permittivity, provide exceptionally high through-thickness permittivity up to 78,000 (≤2.0 MHz), corresponding to a capacitance of 370 μF/m^2. The high capacitance is consistent with the equation for negative and positive capacitors in series. The permittivity tailoring of the composites involves dielectric cellulosic tissue paper interlaminar interlayers. Negative permittivity (not previously reported for carbon fiber composites) requires the paper to be wet with tap water (resistivity 1.5 kΩ cm) during incorporation in the composite, though the water evaporates and leaves ions at very low concentrations during composite fabrication, and also requires optimum through-thickness resistivity (e.g., 1 kΩ cm, as given by paper thickness 35 μm); it is probably due to interactions between the functional groups on the carbon fiber surface and the residual ions (mainly chloride) left after tap water evaporation.

Introduction

Electric permittivity refers to the dielectric polarization behavior, as described by the relative dielectric constant (i.e., the relative permittivity). The permittivity is normally positive (Fig. 1a), but negative permittivity (Fig. 1b) has been reported in special cases. For example, negative permittivity has been reported in graphene with magnetic nanoparticles [1], multiwalled carbon nanotube polyaniline–matrix composites [2], Fe_3O_4 polyaniline–matrix composites [3], nickel–alumina meta-composites [4], perovskite $La_{1-x}Sr_xMnO_3$ [5], copper yttrium-iron-garnet hybrid polyphenylene-sulfide-matrix composites [6], and other materials. Optical, electromagnetic, and magnetic applications are relevant.

Address correspondence to E-mail: ddlchung@buffalo.edu

DOI 10.1007/s10853-016-9979-3

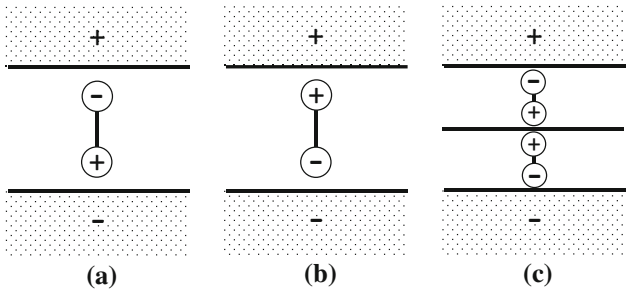

Figure 1 Illustration of **a** positive permittivity, **b** negative permittivity, and **c** positive and negative permittivity components in series electrically. An electric dipole is indicated by + and −, each inside a *circle*, that are connected by a *vertical line*. The + and − signs without encasing *circles* indicate the applied voltage polarity.

Continuous carbon fiber polymer–matrix composites are lightweight structural materials. Their multifunctionality is attractive for smart structures. Functions that have been reported include strain/stress sensing [7], structural health monitoring [8], electric power generation [9, 10], energy storage [11–20], heat dissipation [21], deicing [22], and vibration damping [23]. The attainment of multifunctionality without the embedment or attachment of devices (e.g., strain gages) is particularly attractive. Compared to the use of devices, it gives lower cost, higher durability, and the absence of mechanical property loss.

Energy storage is needed for electric vehicles and self-powered structures. It was first reported in continuous carbon fiber polymer–matrix composites in the through-thickness direction in 2001 by Luo and Chung [11], who reported that the composite with writing paper at the interlaminar interface is a dielectric capacitor in the through-thickness direction with a capacitance of about 1 $\mu F/m^2$. The through-thickness direction is the direction perpendicular to the fibers, which are oriented two dimensionally. Due to the electrical conductivity of the carbon fibers and the non-conductivity of the polymer matrix, this direction provides a configuration that is akin to that of a parallel-plate capacitor.

The effect reported by Luo and Chung [11] was later reported by Carlson et al. [12, 13], who reported in 2013 a capacitance of 450 nF/m^2. Other workers reported the use of carbon fibers to make supercapacitors [14–16] and batteries [17–20]. A dielectric capacitor requires a dielectric material sandwiched by conductive materials. Compared to supercapacitors and batteries, which require electrodes and electrolytes, dielectric capacitors are attractive for their structural simplicity and high-frequency capability. The structural simplicity results in relatively low tendency for the capacitor structure to degrade the mechanical properties of the structural composite. In order to avoid loss in mechanical properties, the fiber volume fraction must remain high. The activation of the fibers, as conducted to increase the fiber surface area [15, 16], tends to degrade the mechanical properties of the fibers.

This paper addresses continuous carbon fiber epoxy–matrix composites that are themselves dielectric capacitors. In contrast to the prior work [11–13], which reports only positive permittivity, this paper reports both positive and negative permittivity, as exhibited by differently formulated composites. Negative permittivity has not been previously reported in carbon fiber composites. Furthermore, this paper reports permittivity values that are much higher in magnitude than prior work.

The permittivity of continuous carbon fiber polymer–matrix composites has been studied by numerous workers at radio wave and microwave frequencies due to the relevance to electromagnetic interference shielding and radar radiation absorption [24–36]. The permittivity reported is all positive.

It is well-known that capacitors can be connected in series or in parallel. In the case of series connection, the capacitance C of the series combination is given by the equation

$$1/C = 1/C_1 + 1/C_2, \tag{1}$$

where C_1 and C_2 are the capacitances of the two capacitors involved. In terms of the relative dielectric constant, Eq. (1) becomes

$$1/\kappa = v_1/\kappa_1 + v_2/\kappa_2, \tag{2}$$

where κ, κ_1, and κ_2 are the values of the relative dielectric constant of the series combination, capacitor 1 and capacitor 2 respectively, and v_1 and v_2 are the volume fractions of capacitors 1 and 2, respectively. However, Eq. (1) and (2) have not been previously applied to the case of C_1 and C_2 being opposite in sign (i.e., κ_1 and κ_2 being opposite in sign), although antiferroelectric ceramics with high values of the relative dielectric constant have been previously reported [37–42]. This paper shows for the first time that Eqs. (1) and (2) are applicable to this case. As a consequence of Eq. (1), C is infinity when C_1 and C_2 are opposite in sign but equal in

magnitude. Indeed, by studying a positive permittivity composite and a negative permittivity composite that are stacked (hence in series) (Fig. 1c), this paper shows that, when C_1 and C_2 are opposite in sign but similar (not exactly equal) in magnitude, the series capacitance per unit geometric area is as high as 370 μF/m^2. As a consequence of Eq. (2), under the condition that v_1/κ_1 and v_2/κ_2 are equal in magnitude but opposite in sign, $1/\kappa$ is zero, which means that κ is infinity. In this paper, v_1/κ_1 and v_2/κ_2 are opposite in sign but similar (not exactly equal) in magnitude, and the resulting series κ is as high as 78,000. The series capacitance or permittivity thus obtained can be exceptional high in magnitude.

This paper is directed at (i) investigating continuous carbon fiber polymer–matrix composites in unprecedented antiferroelectric coupling, (ii) providing carbon fiber polymer–matrix structural composites that exhibit tailored positive and negative permittivities of high magnitudes in the through-thickness direction, (iii) investigating the permittivity of stacked composites with positive and negative permittivities, and (iv) advancing the field of structural capacitors with the ultimate technological goal of large-scale electrical energy storage in structures.

Negative permittivity in combination with negative permeability is attractive for special optical effects such as cloaking that results from negative values of the refractive index. This behavior has been observed in metamaterials [43], which are to be distinguished from monolithic materials. Furthermore, prior work on negative permittivity/permeability materials emphasizes electromagnetic radiation in the radio wave and microwave regimes. This paper concerns monolithic materials at lower frequencies (from 100 kHz to 2.0 MHz). It addresses the permittivity, but does not address the permeability. Negative permeability would require additional tailoring of the composite that is beyond the scope of this work.

Experimental methods

Materials

The composites are carbon fiber epoxy–matrix composite laminates. The fibers are Pyrofil TR50S[1] 15 K unsized PAN-based carbon fibers, with 15,000 filaments in a tow, filament diameter 7 μm, density 1.82 g/cm^3, elastic modulus 240 GPa, tensile strength 4900 MPa, elongation at break 2 %, Poisson's ratio 0.285, and coefficient of thermal expansion 0.5×10^{-6} K^{-1}. The epoxy is a toughened epoxy resin system (TC275), with curing temperature 177 °C (0.1 MPa and 120 min) and density 1.15 g/cm^3. The resin and the carbon fibers are together in the form of prepreg sheets with areal mass 150 ± 5 g/m^2 and resin content (34 ± 2)% (Tencate Advanced Composites, Morgan Hill, CA). The carbon fibers are unidirectional in each lamina, such that the laminae are stacked in the crossply configuration. The number of laminae range from 3 to 11 laminae. At least three thicknesses (corresponding to three different numbers of laminae) are tested for each type of laminate.

The composite contains a soft tissue paper sheet at every interlaminar space. The paper is non-conductive. Three thicknesses (25, 35, and 60 μm) are used. The thickness of 60 μm corresponds to single-ply tissue paper. The thicknesses of 25 and 35 μm correspond to Tosa TENGU chlorine-free Japanese tissue paper,[2] as made from the cellulose fibers of the kozo plant (paper mulberry). The latter paper has thickness (prior to incorporation in the composite) 35 μm, unless noted otherwise. Its mass is 9.0 g/m^2. Its density (including the air in the paper) is 0.242 g/cm^3. With the density of the cellulose fiber in the paper taken as 1.50 g/cm^3 [44], the volume fraction of cellulose fiber in the paper is 16 %. During the paper production, the raw materials (Kozo) are treated with sodium carbonate (approximately 18 wt% relative to the raw materials) in order to remove the binding substances such as pectin and lignin from the fibers.

Table 1 shows that the resistivity is higher for deionized water (8.0 kΩ cm at 1.0 MHz) than tap water (1.5 kΩ cm at 1.0 MHz), while the relative dielectric constant is similar (70 at 1.0 MHz) for deionized water and tap water. The value of 70 is the same as the value previously reported for water at 1 kHz [45]. The difference in resistivity is consistent with the notion that ions that exist in the tap water contribute to electrical conduction. However, the

[1] http://www.fibermaxcomposites.com/shop/datasheets/TR50S_15K_03_2010.pdf, as viewed on May 25, 2015.

[2] http://en.wikipedia.org/wiki/Japanese_tissue, as viewed on May 22, 2015; http://japanese-paper.hidakawashi.com/paper-TENGU/index.html, as viewed on May 22, 2015; https://hiromipaper.wordpress.com/category/about-washi/, as viewed on May 22, 2015.

Table 1 Relative dielectric constant and resistivity of water, standalone paper, paper interlayer material (with epoxy but without carbon fiber), and carbon fiber epoxy–matrix composite with a paper interlayer at every interlaminar space

Material	Paper thickness (μm)	Paper wetness	Relative dielectric constant				Resistivity (kΩ cm)			
			100 kHz	500 kHz	1.0 MHz	2.0 MHz	100 kHz	500 kHz	1.0 MHz	2.0 MHz
Tap water	–	–	(566 ± 187)	91.9 ± 15.0	72.4 ± 5.8	65.9 ± 4.2	1.29 ± 0.03	1.47 ± 0.10	1.47 ± 0.10	1.41 ± 0.09
Deionized water	–	–	(443 ± 205)	84.0 ± 34.7	67.3 ± 27.9	62.2 ± 32.4	7.46 ± 0.54	7.72 ± 0.25	8.00 ± 0.27	8.01 ± 0.33
Standalone paper	25	Wet	1.23 ± 0.05	1.18 ± 0.01	1.19 ± 0.03	1.16 ± 0.02	198 ± 9	37.3 ± 0.8	24.0 ± 1.6	21.1 ± 2.2
		Dried	1.44 ± 0.08	1.30 ± 0.02	1.30 ± 0.01	1.28 ± 0.01	373 ± 31	65.8 ± 6.6	35.9 ± 3.5	28.0 ± 0.1
	35	Extra wet	–	–	16.2 ± 1.4	8.56 ± 1.28	1520 ± 230	899 ± 191	433 ± 110	172 ± 46
		Wet	1.42 ± 0.05	1.33 ± 0.03	1.34 ± 0.04	1.34 ± 0.03	130 ± 18	46.7 ± 1.6	25.7 ± 1.2	20.4 ± 0.9
		As received	1.35 ± 0.04	1.34 ± 0.06	1.32 ± 0.00	1.33 ± 0.01	212 ± 17	38.2 ± 0.1	25.1 ± 0.8	23.2 ± 0.8
		Dried	1.34 ± 0.04	1.37 ± 0.03	1.37 ± 0.03	1.39 ± 0.00	385 ± 19	76.8 ± 7.1	37.6 ± 2.6	26.9 ± 3.5
Paper interlayer material	25	Dried	3.45 ± 0.52	3.17 ± 0.30	3.21 ± 0.06	3.18 ± 0.09	73.9 ± 0.1	15.3 ± 1.5	8.2 ± 0.1	6.4 ± 0.2
	35	Wet	3.11 ± 0.41	3.06 ± 0.26	3.19 ± 0.11	3.16 ± 0.30	235 ± 7	49.2 ± 0.8	28.4 ± 0.6	18.7 ± 0.3
		Dried	3.76 ± 0.11	4.00 ± 0.05	4.08 ± 0.21	3.93 ± 0.20	432 ± 16	68.2 ± 1.5	30.1 ± 0.9	14.8 ± 0.6
Carbon fiber epoxy–matrix composite with paper interlayer	25	Wet	(90.7 ± 67.7)	(310 ± 286)	(−2680 ± 2700)	(−792 ± 817)	0.247 ± 0.020	0.250 ± 0.021	0.254 ± 0.024	0.253 ± 0.026
		As received	−259 ± 41	−257 ± 38	−258 ± 41	−265 ± 45	0.256 ± 0.027	0.248 ± 0.025	0.246 ± 0.033	0.244 ± 0.022
		Dried	−248 ± 99	−143 ± 23	(−284 ± 209)	(−457 ± 438)	0.266 ± 0.002	0.263 ± 0.003	0.262 ± 0.003	0.259 ± 0.002
	35	Extra wet[a]	(50.1 ± 52.8)	(71.5 ± 45.0)	170 ± 38	(113 ± 296)	2.82 ± 0.17	2.82 ± 0.17	2.81 ± 0.18	2.77 ± 0.17
		Extra wet	−596 ± 65	−500 ± 50	−548 ± 47	−538 ± 14	1.38 ± 0.18	1.38 ± 0.17	1.38 ± 0.18	1.37 ± 0.17
		Wet	−204 ± 69	−187 ± 43	−161 ± 20	−154 ± 11	1.49 ± 0.07	1.49 ± 0.07	1.49 ± 0.07	1.47 ± 0.07
		As received	−102 ± 12	−101 ± 13	−102 ± 16	−99.2 ± 8.6	1.90 ± 0.02	1.89 ± 0.03	1.89 ± 0.03	1.86 ± 0.02
		Dried	425 ± 46	313 ± 16	217 ± 41	149 ± 77	2.12 ± 0.18	2.01 ± 0.13	2.01 ± 0.14	1.98 ± 0.14
	60	Wet	39.6 ± 0.7	28.4 ± 3.1	20.6 ± 1.2	17.1 ± 0.9	160 ± 50	53.2 ± 1.2	32.7 ± 1.4	17.3 ± 6.0
		As received	27.3 ± 13.8	15.3 ± 3.6	13.5 ± 1.5	13.5 ± 0.5	156 ± 40	84.5 ± 8.1	39.8 ± 2.6	15.3 ± 4.1

The wet paper and extra wet paper involve tap water, unless noted otherwise. The ± ranges for the relative dielectric constant are obtained by fitting the plot of $1/C_m$ versus thickness with various straight lines and determining the range of slope from these lines. The ± ranges for the resistivity are obtained by fitting the plot of R_m versus thickness with various straight lines and determining the range of slope from these lines. The values in parentheses have large ± ranges, due to the inadequate linearity in the plot

[a] Deionized water

relatively large error in the relative dielectric constant makes the difference, if any, in relative dielectric constant between tap water and deionized water. The main contaminants in the tap water are chloride (20 mg/L, or 0.002 wt% chloride), fluoride (0.96 mg/L), and nitrate (0.06 mg/L) and the average pH of the tap water is 7.84, according to the Erie County Water Authority that supplies the tap water.[3] Unless stated otherwise, the water used in this work is tap water. X-ray spectroscopic elemental analysis (in conjunction with scanning electron microscopy) shows that the tap water contains calcium and silicon (with calcium being twice as abundant as silicon in atomic scale rather than mass scale), which are absent in deionized water.

The tissue paper is allowed to contain different amounts of either tap or deionized water. For each type of paper, the water content is controlled at up to four levels, which are referred to as the dried, as-received, wet, and extra wet states, as listed in the order of increasing wetness. The dried state is obtained by drying the as-received paper at 110 °C for 1.0 h, such that the dried paper is used immediately after the period of drying. The wet state is obtained by exposing the dried paper to the moisture above the water that is contained in a closed glass container for 20 h, such that the wet paper is used immediately after removal from the moisture container. The extra wet state is obtained by immersion in water, followed by removal from the water and partial drying at room temperature for a controlled time, which is chosen to provide the water content desired, i.e., 50 % increase in weight relative to the dried state. For the 35-μm-thick paper, the weight increase is (20 ± 2)% for the wet state relative to the dried state, and (5.5 ± 1.1)% for the as-received state relative to the dried state; this means that the weight increase is (15 ± 1)% for the wet state relative to the as-received state. For the 25-μm-thick paper, the weight increase is (20 ± 3)% for the wet state relative to the dried state and is (4.5 ± 1.5)% for the as-received state relative to the dried state; this means that the weight increase is (16 ± 2)% for the wet state relative to the as-received state. For the 60-μm-thick paper, the weight increase is (25 ± 2)% for the wet state relative to the dried state and is (3.0 ± 0.8)% for the as-received state relative to the dried state; this means that the weight increase is (21 ± 2)% for the wet state relative to the as-received state.

In order to investigate the origin of the results obtained for the laminates with the paper interlayers, the interlayer material (paper impregnated with epoxy) in the absence of carbon fibers is also studied. The resin used for the interlayer materials is EPON Resin 813[4] with EPICURE 3234 curing agent.[5] Both from Hexion, such that the ratio of resin to curing agent is 100:13 by mass. The epoxy resin (with curing agent) in the amount of 0.1 g (as controlled by using a pipette) was introduced to each of the two sides of a single sheet of the paper (25.4 × 25.4 mm, i.e., 1.0 × 1.0 in). The desired number of sheets are then stacked and then placed between PTFE sheets, followed by curing of the resin by hot pressing at 100 °C and 0.1 MPa for 1.0 h. The curing conditions are as recommended by the manufacturer. Excessive epoxy resin was squeezed out during the curing.

Each type of paper is tested (i) in the absence of epoxy or carbon fiber (with different thicknesses provided by simply stacking of different numbers of sheets of the paper), (ii) in the presence of epoxy (type TC275[6] with density 1.15 g/cm^3), but no carbon fiber (with different thicknesses provided by stacking different numbers of the epoxy-impregnated paper sheets prior to the curing of the epoxy), and (iii) in the presence of carbon fiber–epoxy prepreg (with different thicknesses provided by stacking different numbers of prepreg sheets prior to the curing of the epoxy). For the paper with the carbon fiber–epoxy prepreg, the paper is incorporated in the crossply prepreg stack, being positioned at every interlaminar interface, prior to consolidation and curing at 177 °C and 0.1 MPa for 120 min. Thus, a 3-lamina composite [0/90/0] has 2 sheets of paper; a 5-lamina composite [0/90/0/90/0] has 4 sheets of paper; a 7-lamina composite [0/90/0/90/0/90/0] has 6 sheets of paper.

Relative dielectric constant measurement

The relative dielectric constant (the real part of the relative permittivity) is obtained by measuring the capacitance of the specimen between copper plate

[3] https://www.ecwa.org/wqreport.pdf, as viewed on May 22, 2015.

[4] https://www.hexion.com/Products/TechnicalDataSheet.aspx?id=2759, as viewed on May 22, 2015.

[5] http://www.miller-stephenson.com/assets/1/Store%20Item/curing%20agents.pdf, as viewed on May 22, 2015.

[6] http://www.tencate.com/emea/Images/TC275-1_DS_101113_Web28-24442.pdf, as viewed on May 22, 2015.

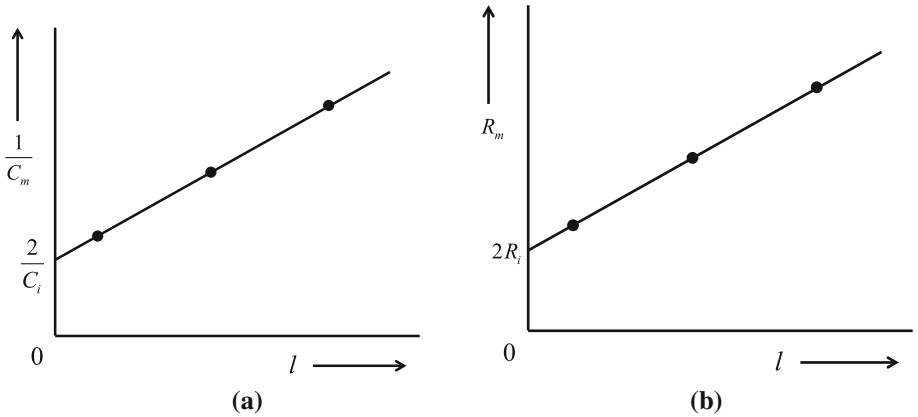

Figure 2 Schematic plots. In the horizontal axis, l is the thickness of the specimen. **a** Plot of $1/C_m$ versus l, for the determination of C_i and κ based on Eq. (3), where C_i is the capacitance of a specimen-contact interface and κ is the relative dielectric constant of the specimen. The slope equals $1/(\varepsilon_0\kappa A)$. The intercept on the vertical axis equals $2/C_i$. **b** Plot of R_m versus l for the determination of R_i and R_s based on Eq. (3). The slope equals the specimen resistance R_s per unit thickness. The intercept on the vertical axis equals two times the resistance R_i of the specimen-contact interface.

electrodes (5.0 mm thick), such that there is an electrically insulating Teflon sheet positioned between the specimen and each copper electrode. A pressure of 15 kPa is applied to the stack in the direction perpendicular to the plane of the stack. Both specimen and electrodes are square, with dimensions 25.4 × 25.4 mm. The capacitance is measured using a precision RLC meter (QuadTech Model 7600), with the electric field across the thickness of the specimen fixed at 3.2 V/cm. The frequencies include 100 kHz, 500 kHz, 1.0 MHz, and 2.0 MHz.

For each type of material tested, specimens at ≥3 thicknesses are tested. The measured capacitance C_m is for the specimen with inclusion of the effect of the two interfaces between the specimen and the two contacts. The two interfaces and the specimen are in series electrically. Hence,

$$1/C_m = 2/C_i + 1/C_v, \quad (3)$$

where C_i is the capacitance due to a specimen-contact interface, $C_v = l/(\varepsilon_0\kappa A)$ is the volumetric capacitance due to the specimen, ε_0 is the permittivity of free space (8.85 × 10^{-12} F/m), κ is the relative dielectric constant of the specimen, A is the contact area, which is the same as the specimen area (25.4 × 25.4 mm), and l is the thickness of the specimen. C_i should be high in order for it to have little influence.

According to Eq. (3), $1/C_m$ is plotted against l, as illustrated in Fig. 2a. The value of C_i is obtained from the intercept of $2/C_i$ at the $1/C_m$ axis at $l = 0$, and the value of κ is obtained from the slope, which is equal to $1/(\varepsilon_0\kappa A)$. The slope equals $1/(\varepsilon_0\kappa A)$, where κ is the relative dielectric constant, A is the area, and ε_0 is the permittivity of free space. This method involving multiple thicknesses allows decoupling of the volumetric and interfacial capacitances [45]. It is in contrast to the conventional method, which involves the testing of a single thickness and considers the measured sum of the volumetric and interfacial capacitances to be the specimen capacitance.

All prior work (other than the recent work by Chung et al. on electrochemical electrodes [45–47]) did not conduct the abovementioned decoupling. In particular, impedance spectroscopy, which measures the impedance as a function of frequency, does not allow this decoupling. Furthermore, the use of an equivalent electrical circuit to analyze the Nyquist plot obtained by impedance spectroscopy for the purpose of determining the resistance and capacitance does not give a direct measurement of the resistance and capacitance and the results of the analysis are dependent on the circuit model chosen.

The negative permittivity reported here is based on the negative slope of the plot of the inverse of the measured capacitance versus the specimen thickness. It is not based on the testing of one thickness, which is what prior work entails. It is also not based on a single permittivity or capacitance value that is read from a meter. Therefore, the negative permittivity reported here is well supported experimentally.

The method used in this paper is very classical, involving a parallel-plate capacitor configuration.

However, this paper pushes this classical method a step further by measuring at three specimen thicknesses, so that the volumetric and interfacial contributions to the measured resistance get decoupled.

The relative dielectric constant determination for water [45] involves (i) measurement of the values of the relative dielectric constant of dry paper towel and the paper towel that has been soaked with the water, and (ii) determination of the volume fraction of air in the dry paper towel by measuring the bulk density of the dry towel and the true density (density of the solid part) of the dry towel. The capacitance C_m is measured for stacks of dry/wet paper towel consisting of one, two, and three pieces of the paper towel. From the slope of the plot of $1/C_m$ versus thickness, the relative dielectric constant of the dry/wet towel is obtained. By using the volume fraction of water in the towel, the Rule of Mixtures, and the relative dielectric constant of the solid part of the paper towel (as deduced from that of the dry towel), the relative dielectric constant of the water is obtained.

Electrical resistivity measurement

The AC resistance is measured in the absence of an insulating film between the specimen and the copper contact. Other than this absence, the configuration is the same as that for relative dielectric constant measurement ("Relative dielectric constant measurement" section). The same RLC meter, AC voltage and frequencies are used.

The measured resistance R_m between the two copper contacts that sandwich the specimen includes the volume resistance R_s of the specimen and the resistance R_i of each of the two interfaces between the specimen and a copper contact, i.e.,

$$R_m = R_s + 2R_i. \quad (4)$$

By measuring R_m at three specimen thicknesses, the curve of R_m versus thickness l is obtained (Fig. 2b). The intercept of this curve with the vertical axis equals $2R_i$, whereas the slope of this curve equals R_s/l, where R_s is the specimen resistance for the specimen thickness of l. The specimen resistivity is obtained by multiplying R_s/l by the specimen area A. This method involving multiple thicknesses allows decoupling of the volumetric and interfacial capacitances [45].

The resistivity determination for water [45] involves measurement of the values of the volume resistivity of the dry paper towel and the paper towel that has been soaked with water. The resistance R_m is measured for stacks of dry/wet paper towel consisting of one, two, and three pieces of the paper towel. From the slope of the plot of R_m versus thickness, the volume resistivity of the dry/wet towel is obtained. The resistivity of the liquid in the towel is calculated from that of the wet towel based on the Rule of Mixtures.

Results and discussion

Material architecture

The wet paper and extra wet paper mentioned in this section involve tap water. However, the material architecture is similar for tap water and deionized water.

First, consider the case of the standalone paper (without epoxy or carbon fiber). The relative dielectric constant of the dried 35-μm paper (with inclusion of the air in the paper) is 1.34 ± 0.04, 1.37 ± 0.03, 1.37 ± 0.03, and 1.39 ± 0.00 at 100 kHz, 500 kHz, 1.0 MHz, and 2.0 MHz, respectively (Table 1). With the standalone paper consisting of 16.1 vol. % cellulose fibers and 83.9 vol% air (based on the measured paper density), the relative dielectric constant of the cellulose fibers in the paper is found to be 3.11 ± 0.25, 3.29 ± 0.19, 3.29 ± 0.19, and 3.42 ± 0.00 at 100 kHz, 500 kHz, 1.0 MHz, and 2.0 MHz, respectively, as calculated based on the Rule of Mixtures for components in parallel.

Next, consider the paper interlayer inside the carbon fiber composite. The interlayer consists of the paper, epoxy, and air. Its volume I is given by

$$I = P + E + A, \quad (5)$$

where A, E, and P are the volume of the air, epoxy, and paper (excluding air) respectively. Let v_a be the volume fraction of air in the paper interlayer (which is inside the carbon fiber composite). Based on Eq. (5),

$$v_a = \frac{A}{I} = \frac{A}{P + E + A}. \quad (6)$$

Image analysis of four carbon fiber composite cross-sectional optical micrographs (at 10×

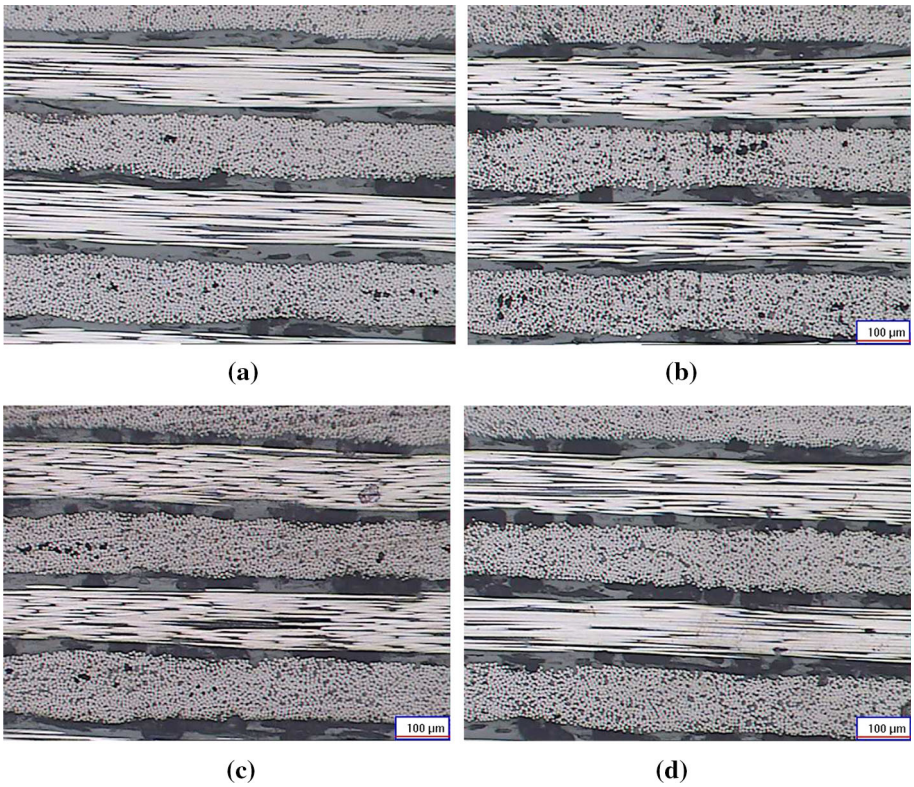

Figure 3 Cross-sectional optical microscope photographs of the mechanically polished edge (plane containing the through-thickness direction). **a** Dried, **b** as received, **c** wet, **d** extra wet.

Table 2 Interlayer material information

Paper wetness degree	Standalone paper interlayer[a]		Paper interlayer in fiber composite				
	Thickness/layer (μm)	Density (g/cm^3)	Thickness t (μm)	Density[b] (g/cm^3)	v_a	v_e	v_p
Dried	34.7	1.10	28.6 ± 1.3	1.34 ± 0.06	0.227 ± 0.016	0.563 ± 0.006	0.210 ± 0.010
As received	35.0	1.09	28.5 ± 1.6	1.34 ± 0.07	0.301 ± 0.051	0.488 ± 0.039	0.211 ± 0.012
Wet	35.3	1.07	28.2 ± 1.6	1.34 ± 0.07	0.491 ± 0.026	0.296 ± 0.013	0.213 ± 0.012
Extra wet	35.5	1.06	28.3 ± 1.4	1.33 ± 0.07	0.615 ± 0.016	0.173 ± 0.005	0.212 ± 0.011
Extra wet[c]	35.0	1.05	28.4 ± 1.9	1.31 ± 0.09	0.587 ± 0.053	0.201 ± 0.039	0.212 ± 0.014

The paper thickness prior to incorporation in the carbon fiber composite is 35 μm. The water is tap water, unless noted otherwise. The volume fractions are relative to the volume of the paper interlayer when the interlayer is in the carbon fiber composite

[a] Not as a part of the carbon fiber composite

[b] Calculated from the measured density of the paper interlayer material by scaling in accordance with the measured thickness, which is smaller for the interlayer inside the fiber composite than the standalone paper interlayer

[c] Deionized water

magnification) is conducted for each level of wetness in order to determine the fraction of the interlayer area that is occupied by air voids, which appear as ~30-μm gray patches in each micrograph, such that the void size is comparable to the interlayer thickness. Figure 3 shows one of the four micrographs for each level of wetness. Based on the image analysis, v_a is determined (Table 2). The size of the air voids in the through-thickness direction is equal to the interlayer thickness for all the wetness levels, though the abundance of air voids increases with increasing wetness level.

The volume of the paper interlayer I in the carbon fiber composite is given by

$$I = t_i l w, \tag{7}$$

where t_i, l, and w are the thickness, length, and width of the paper interlayer in the carbon fiber composite.

The volume of the paper (excluding air) in the paper interlayer (inside the composite) is given by

$$P = \frac{l w t_p \alpha_{pa}}{\alpha_p}, \tag{8}$$

where t_p is the thickness of the paper prior to incorporation in the carbon fiber composite (typically 35 μm in this work), α_{pa} is the density of the standalone paper (including air), with $\alpha_{pa} = 0.257$ g/cm^3 (as measured in this work), and α_p is the density of the standalone paper (excluding the air), with $\alpha_p = 1.50$ g/cm^3 [44]. In the right side of Eq. (8), the numerator is the mass of the cellulose fibers in the paper.

The volume fraction v_e of the epoxy in the paper interlayer (inside the carbon fiber composite), based on Eq. (5), is given by

$$v_e = \frac{E}{I} = \frac{E}{P + E + A} \tag{9}$$

and is calculated using Eq. (9) based on the values of E, P, and A determined by image analysis. The volume fraction v_p of the paper (excluding the air) in the paper interlayer (inside the carbon fiber composite), based on Eq. (5), is given by

$$v_p = \frac{P}{I} = \frac{P}{P + E + A} \tag{10}$$

and is calculated using Eq. (10) based on the values of P (from Eq. 8), E, and A.

Table 2 shows that the density and thickness of the paper interlayer, whether standalone or as a part of the carbon composite, is essentially independent of the degree of wetness. This supports the expected occurrence of water evaporation during the 177 °C curing of the composite. The thickness of the paper interlayer in the carbon fiber composite is smaller than that of the standalone paper. This is attributed to the consolidation during the hot pressing in the carbon fiber composite fabrication.

As shown in Table 2, the volume fraction v_p of the paper (excluding the air) is essentially independent of the degree of wetness, but the volume fraction v_a of the air increases and the volume fraction v_e of the epoxy decreases with increasing degree of wetness. The volume fraction v_p of the paper (excluding the air) is lower than or comparable to the volume fraction v_a of the air for all of the degrees of wetness. In addition, v_p is lower than or comparable to v_a for all of the degrees of wetness. In particular, the paper is the most minor constituent for all degrees of wetness other than the extra wet case. The epoxy is the most major constituent for the dried and as-received cases, but the air is the most major constituent for the wet and extra wet cases.

Table 3 shows the material architectural information for the carbon fiber epoxy–matrix composites with and without interlayer. The constituent volume fractions are based on cross-sectional optical microscopic examination, in addition to calculation involving the Rule of Mixtures for the composite density. The carbon fiber volume fraction is reduced slightly by the presence of the interlayer, such that it is slightly lower for the 35-μm paper interlayer than the 25-μm interlayer, as expected. The cellulose fiber volume fraction (the cellulose fiber being in the paper) is higher for the 35-μm interlayer than the 25-μm paper interlayer, as expected. The air volume fraction is also higher for the 35-μm interlayer than the 35-μm paper interlayer, such that it is higher for the extra wet case than the dried case for the same thickness of paper, as expected from the fact that the air is associated with the interlayer. The epoxy volume fraction is reduced by the presence of the interlayer, such that it is lower for the extra wet case than the dried case for the same thickness of paper, as expected from the fact that the air volume fraction is higher for the extra wet case than the dried case.

Positive and negative permittivity behavior

Using tap water

The wet paper and extra wet paper mentioned in this section involve tap water. As shown in Table 1, the relative dielectric constant is positive and small for the standalone paper of all thicknesses and wetness levels and at any of the frequencies (without epoxy or carbon fiber). Except for the extra wet case, the values are all below 1.4 and essentially do not depend on the degree of wetness. For the extra wet case, the relative dielectric constant is much higher, reaching 16 at 1.0 MHz. The linearity of the plot of the reciprocal of the measured capacitance versus the thickness is excellent in all cases (Fig. 4).

The paper interlayer material (paper with epoxy, not as a part of the carbon fiber composite) exhibits

Table 3 Carbon fiber composite architecture

Interlayer	Density (g/cm^3)	Volume fraction			
		Carbon fiber	Epoxy	Cellulose fiber	Air
None	1.538 ± 0.010	0.564 ± 0.015	0.436 ± 0.015	–	–
Dried 25 μm	1.535 ± 0.005	0.518 ± 0.014	0.432 ± 0.065	0.021 ± 0.002	0.028 ± 0.011
Extra wet 25 μm	1.536 ± 0.007	0.523 ± 0.014	0.408 ± 0.085	0.021 ± 0.002	0.047 ± 0.017
Dried 35 μm	1.514 ± 0.017	0.489 ± 0.012	0.420 ± 0.108	0.035 ± 0.001	0.056 ± 0.020
Extra wet 35 μm	1.488 ± 0.011	0.491 ± 0.013	0.373 ± 0.155	0.035 ± 0.001	0.101 ± 0.027

The composite density and the volume fractions of carbon fiber, epoxy, cellulose fiber, and air in carbon fiber epoxy–matrix composites with various interlayers are shown. The water is tap water. In contrast to Table 2, the volume fractions are relative to the volume of the carbon fiber composite

positive values of the relative dielectric constant, such that the values are higher than those of the corresponding standalone paper (without epoxy) (Table 1). This means that the epoxy contributes to the permittivity, such that it causes the permittivity to be more positive.

The carbon fiber composite with paper interlayer exhibits positive or negative values of the relative dielectric constant, such that the magnitude is much higher than that of the corresponding paper interlayer material (with epoxy, but without carbon fiber) or the corresponding standalone paper. The linearity of the plot of $1/C_m$ versus thickness is excellent for almost all cases (Figs. 4, 5). Linearity means that the contribution of the interlaminar interfaces to $1/C_m$ is negligible compared to the contribution of the laminae to $1/C_m$, as explained in "Negligible contribution of the interlaminar interface to the dielectric or conduction behavior" section. The cases of poor linearity are at least partly due to the contribution of the interlaminar interfaces to $1/C_m$ being not negligible compared to the contribution of the laminae to $1/C_m$.

For carbon fiber composites with the 35-μm paper, the relative dielectric constant is positive for the dried state and is negative for the as-received, wet, and extra wet states, such that the value becomes more negative as the degree of wetness increases (Table 1). This trend is observed at any of the frequencies. For the extra wet state, the relative dielectric constant is as negative as −600; for the wet state, it is as negative as −200; for the as-received state, the value is −100. This indicates that the wetness promotes the negative permittivity. Since the paper interlayer material (with epoxy, not as a part of the carbon fiber composite) does not give negative permittivity, the origin of the negative permittivity involves the carbon fibers, probably the functional groups (e.g., hydroxyl, carbonyl, and carboxylic groups [48]) on the surface of the carbon fibers. Such an effect of the surface functional groups has been shown for various carbon materials [45, 46]. The wetness promotes this effect, probably due to the interaction of residual adsorbed ionic species with the functional groups. As shown in Table 1, negative permittivity is found in five different types of composite. The magnitude of the relative dielectric constant tends to decrease with increasing frequency, as expected.

For the carbon fiber composites with the 25-μm paper, the relative dielectric constant is negative for the as-received and dried states, but is positive (though not very clear due to the inadequate linearity of the plot of $1/C_m$ versus thickness) for the wet state. For the as-received state, the relative dielectric constant is −260, with good linearity (Fig. 4). For the dried state, the value is not as clear, due to the inadequate linearity. Compared to the composites with the 35-μm paper, the linearity tends to be not as good and the values of the relative dielectric constant tend to be not as accurate.

For the composites with the 60-μm paper, the relative dielectric constant is positive for both wetness levels, and the linearity is good (Fig. 4 for the as-received state). It appears that negative permittivity cannot occur when the interlaminar interface thickness is too large (60-μm paper). The intermediate thickness given by the 35-μm paper appears to be optimum for giving negative permittivity.

The most positive permittivity, with the relative dielectric constant up to 400, is exhibited by the composite with 35-μm dried paper. The cellulose fibers in the paper have relative dielectric constant 3 only ("Material architecture" section). The value of

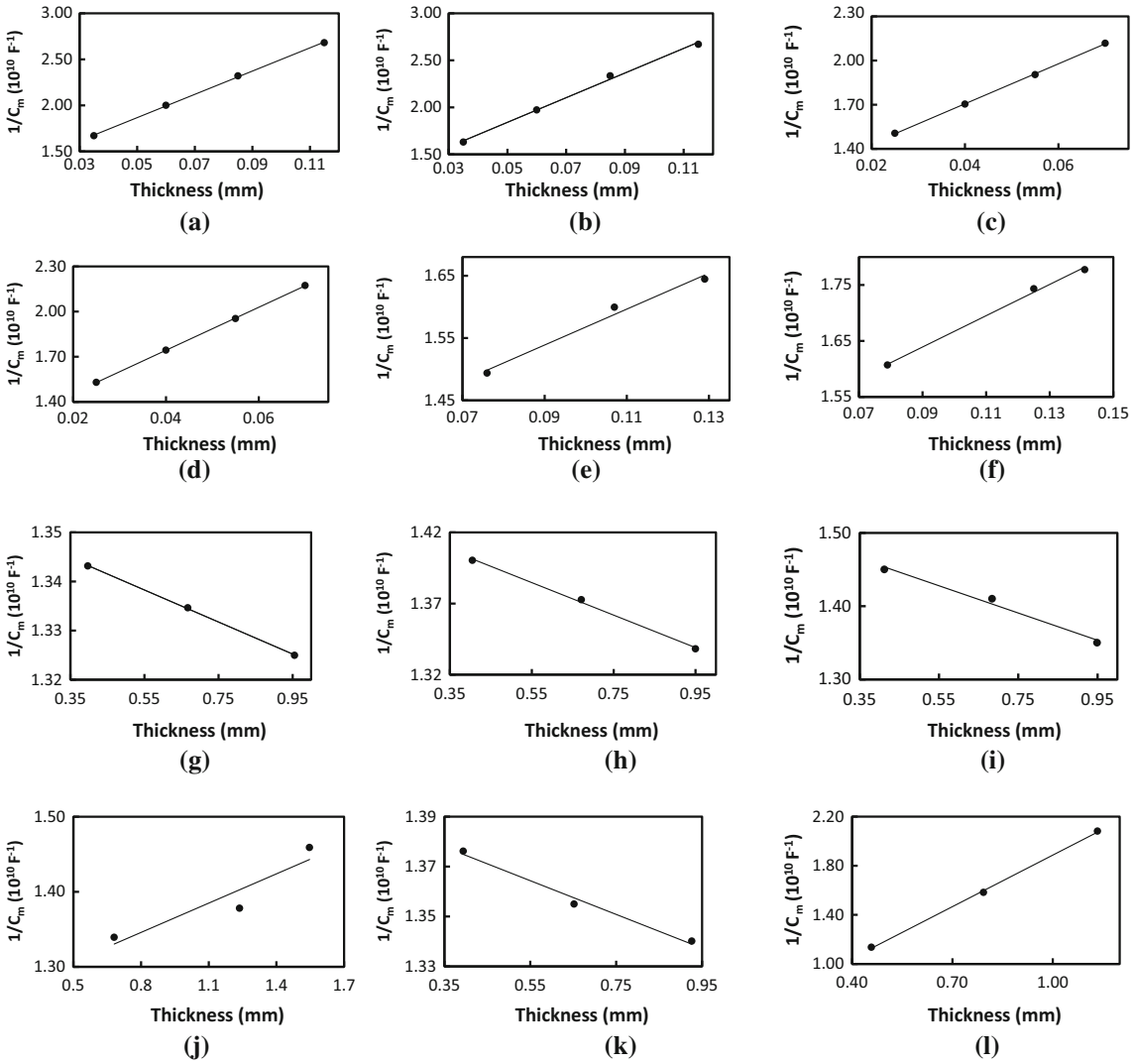

Figure 4 Plot of $1/C_m$ (2.0 MHz) versus the specimen thickness. The plot is in accordance with Eq. (3). **a** Standalone dried 35-μm-thick paper. **b** Standalone wet 35-μm-thick paper. **c** Standalone dried 25-μm-thick paper. **d** Standalone wet 25-μm-thick paper alone. **e** Paper interlayer material (with epoxy but without carbon fiber) in the dried state for the paper. **f** Paper interlayer material (with epoxy but without carbon fiber) in the wet state for the paper. The three thicknesses of paper interlayer material correspond to stacks of 2, 3, and 4 sheets of paper of thickness 35 μm; the thickness of the stack with 3 sheets is consistently much greater than that of the stack with 2 sheets for the wet case. **g** Carbon fiber composite with the extra wet 35-μm-thick paper. **h** Carbon fiber composite with the wet 35-μm-thick paper. **i** Carbon fiber composite with the as-received 35-μm-thick paper. **j** Carbon fiber composite with the dried 35-μm-thick paper. **k** Carbon fiber composite with the as-received 25-μm-thick paper. **l** Carbon fiber composite with the as-received 60-μm-thick paper.

400 is much more positive than the most positive value (20 [11]) previously reported for a carbon fiber composite, which is one with barium titanate particles as the interlayer. At 2 MHz, the relative dielectric constant of a carbon fiber composite with barium titanate particles as the interlayer is 19.8 [11], compared to the value of 149 at the same frequency for the composite of this work with 35-μm-dried paper. Barium titanate is well-known for its high positive value of the relative dielectric constant (e.g., 4300 [49]). In the absence of carbon fiber or epoxy, the values are less positive. Thus, the high positive values of up to 400 are probably due to the interaction between the functional groups on the carbon fiber surface and some residual ions in the dried paper after the tap water has evaporated. The quantity of

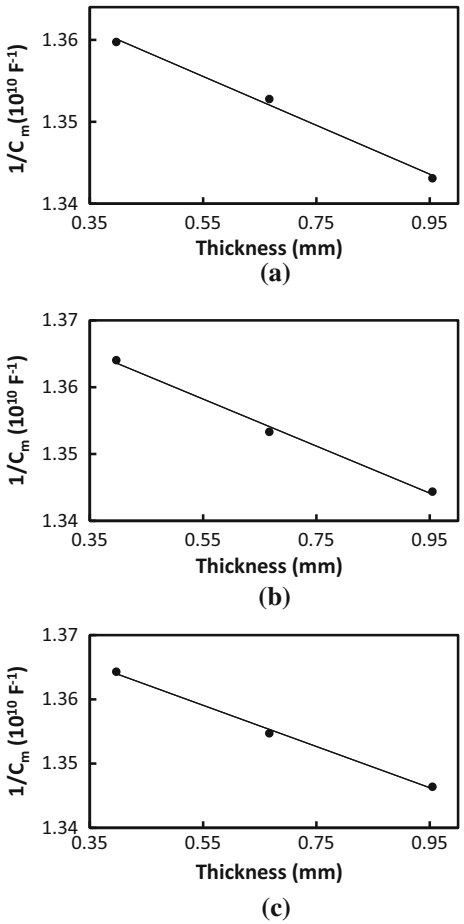

Figure 5 Plot of $1/C_m$ at various frequencies versus the specimen thickness. The plot is in accordance with Eq. (3). The specimen is extra wet 35-μm-thick paper carbon fiber composite. **a** 100 kHz. **b** 500 kHz. **c** 1.0 MHz.

the residual ions is likely smaller for the dried paper than the wet or extra wet paper, even though the wet or extra wet paper has been effectively dried during the hot pressing in composite fabrication. Due to the dryness, no liquid electrolyte is present and the capacitor associated with the permittivity is thus not electrochemical in nature. In order for the permittivity to be negative, the interaction probably needs to be strong enough, as provided by a larger quantity of residual ions.

Using deionized water

The extra wet paper used in this section for the carbon fiber epoxy–matrix composite involves deionized water. The relative dielectric constant of the carbon fiber composite (Table 1) is positive at all frequencies, with values 50 ± 53, 72 ± 45, 170 ± 38, and 113 ± 296 at 100 kHz, 500 kHz, 1.0 MHz, and 2.0 MHz, respectively. This means that the negative values obtained in "Using tap water" section using tap water stem from the residual ions that remain after the evaporation of the tap water.

Using deionized water with dissolved ions

The use of deionized water with intentionally dissolved sodium carbonate (0.01 wt% aqueous solution), the resulting carbon fiber epoxy–matrix composite exhibits positive permittivity. However, the use of water with intentionally dissolved sodium chloride (0.01 wt% aqueous solution) or nickel sulfate hexahydrate (0.05 and 4.5 wt% aqueous solutions) gives carbon fiber composites with very large data scatter of the permittivity, so that even the sign of the permittivity is unclear.

The dominant ions in the tap water are associated with chloride at 0.002 wt%, which is much lower in concentration than the abovementioned intentionally dissolved ions. Thus, a very low ionic concentration seems to be necessary for the occurrence of negative permittivity. Further work is needed to determine the requirements regarding the type and concentration of the ions.

Electrical resistivity of positive and negative permittivity materials

As shown in Table 1, for the standalone 35-μm paper, the trend of the resistivity decreasing with increasing wetness applies to the lowest frequency of 100 kHz when the extra wet case is excluded. For the extra wet case, the resistivity is much higher than the wet case for any of the frequencies. This means that a high proportion of water (as in the extra wet case) is detrimental to the conduction at any of the frequencies, whereas a low proportion of water (as in the wet and as-received cases) helps the conduction. This suggests that the cellulose fiber in the paper contributes significantly to conduction by electronic conduction, which is hindered when a large amount of water present decreases the continuity of the electronic conduction path provided by the cellulose fiber. On the other hand, when an intermediate amount of water is present (as in the wet and as-received cases), the water is not enough to affect the continuity of the electronic conduction path provided by the cellulose fiber, while it provides an ionic

conduction path that coexists with the electronic conduction path provided by the fiber. As a result, when a medium amount of water is present, the water helps the conduction.

For the standalone 35-μm paper, when the extra wet case is excluded, the resistivity is essentially independent of the wetness at the highest frequency of 2.0 MHz, indicating that water essentially does not contribute to the conduction at this high frequency. At the intermediate frequencies of 1.0 MHz and 500 kHz, the resistivity decreases from the dried case to the as-received case, but increases from the as-received case to the wet case and further increases from the wet case to the extra wet case, indicating that a low degree of wetness (as in the as-received case) helps the conduction whereas a high degree of wetness (as in the wet and extra wet cases) hinders the conduction. This means that water contributes to the conduction at these intermediate frequencies for the as-received case, such that the contribution is less than that at the lowest frequency of 100 kHz and is higher than that at the highest frequency of 2.0 MHz. In other words, the electronic conduction due to the cellulose fiber plays a significant role in the conduction at all frequencies, such that its contribution relative to the ionic conduction contribution by water increases with increasing frequency.

For the standalone 25-μm paper, Table 1 shows that the resistivity decreases with increasing wetness from the dried case to the wet case at all frequencies, although the effect becomes weaker as the frequency increases. This means that ionic conduction due to the water contributes to the conduction in the 25-μm paper for the wet case. Since the extra wet case is not included in the investigation of the 25-μm paper, data are not adequate for assessing the relative contributions of the ionic conduction due to water and the electronic conduction due to the cellulose fibers for the case of the 25-μm paper.

For the carbon fiber composite with 35-μm paper interlayer (Table 1), the resistivity monotonically decreases with increasing wetness (from the dried case to the extra wet case) at all frequencies. This means that the wetness promotes conduction. Since the water has evaporated away during the composite fabrication, the effect of wetness is attributed to the residual adsorbed ionic species left after the water evaporation. This notion is supported by the result that the resistivity is much higher for the carbon fiber composite (extra wet case) with deionized water than that with tap water (Table 1).

Electronic conduction is significant in the standalone paper (without evaporation of the water), as discussed above in relation to the standalone 35-μm paper. With the water having evaporated in the carbon fiber composite, electronic conduction is expected to be even more important—to the extent that the conduction is essentially all electronic. This is consistent with the result that the resistivity of the carbon fiber composite with extra wet paper interlayer is comparable to that with wet paper interlayer, whereas, for the standalone paper, the resistivity is much higher for the extra wet case than the wet case. Since the water has evaporated in the carbon fiber composite, it is not available to hamper the electronic conduction path, even in the extra wet case. Nevertheless, the residual ions left after the water evaporation contribute slightly to ionic conduction, as suggested by the result that the resistivity of the carbon fiber composite decreases slightly with increasing wetness of the paper interlayer (Table 1).

For the same wet state, the carbon fiber composite with a thinner paper interlayer gives a lower resistivity, as shown by the progressive decrease in resistivity from 60 to 35 and to 25-μm paper thickness (Table 1). This is expected, because the thicker paper makes it more difficult for the carbon fibers in one lamina to touch those of an adjacent lamina. Figure 6 shows the linearity of the plots of the measured resistance versus the specimen thickness.

The degree of fiber–fiber contact across the interlaminar interface plays a role in affecting the through-thickness electrical conduction of carbon fiber laminates. A high degree of fiber–fiber contact is reflected by a low value of the contact electrical resistivity of the interlaminar interface [50, 51]. Probably the resistivity is too low for the composite with the 25-μm paper, so that the negative permittivity cannot occur. Probably the resistivity is too high (or the fiber–fiber contact too little) for the composite with the 60-μm paper, so that the negative permittivity cannot occur. The thickness of 35 μm is apparently optimum for giving the needed conduction behavior for providing negative permittivity in the carbon fiber composite.

Figure 7 illustrates a plausible (tentative) mechanism for the negative permittivity. The functional groups on a carbon fiber are oriented due to electrostatic interaction with the applied electric field, thus resulting in positive permittivity (Fig. 7a). The

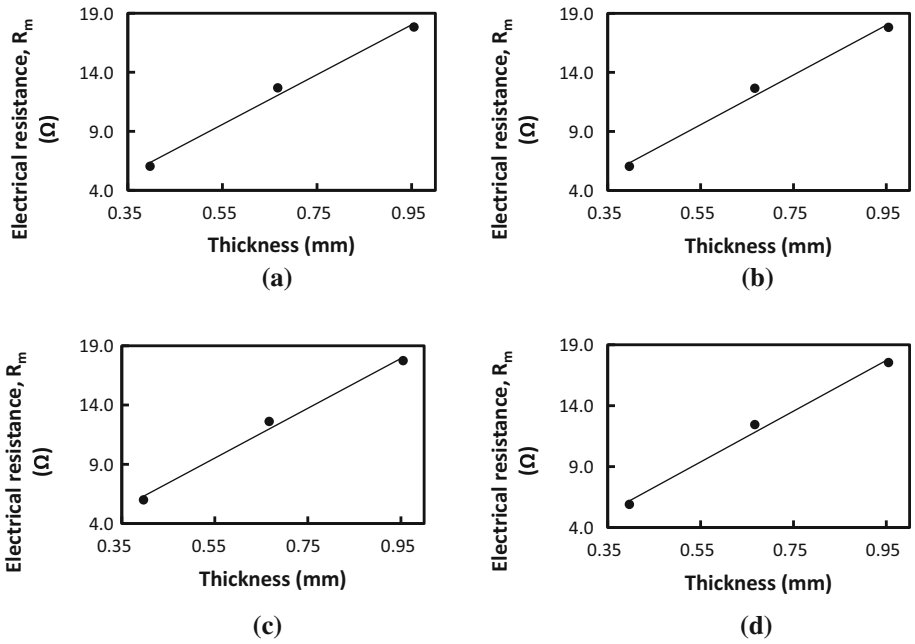

Figure 6 Plots of the measured resistance R_m versus thickness of extra wet 35-μm paper carbon fiber composite at various frequencies. The plots are in accordance with Eq. (4). **a** 100 kHz. **b** 500 kHz. **c** 1.0 MHz. **d** 2.0 MHz.

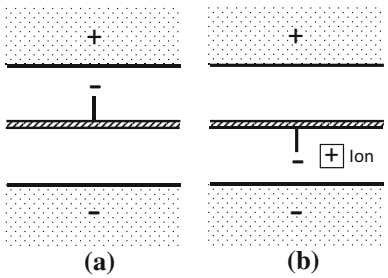

Figure 7 Illustration of a plausible (tentative) mechanism of **a** positive permittivity and **b** negative permittivity in carbon fiber composite. The *dotted regions* at the *top* and *bottom* represent electrodes for providing the applied electric field. The + and − signs in these regions indicate the applied voltage polarity. The *horizontal shaded region* at the center represents a part of a carbon fiber. The *vertical bold line* emanating from the fiber represents a polar functional group on the fiber surface. A cation rather than an anion is shown in **b**, as indicated by a + sign encased in a square, because cations tend to be smaller and hence more mobile than anions.

residual ions (from the tap water) are mobile to a limited degree and move slightly in response to the applied electric field. These ions also interact electrically with the functional groups, thereby resulting in negative permittivity (Fig. 7b).

For an ideal capacitor with no energy loss, the resistance should be infinity. The resistivity (e.g., 2.8 kΩ cm for the carbon fiber composite with extra wet paper, Table 1) is too low for achieving a lossless capacitor. This issue may be alleviated in practice by adding an electrically insulating film, such as a thin plastic film, at the interface between the composite and the electrical contact.

Positive and negative permittivity components electrically in series

Permittivity behavior

For two volumes (labeled 1 and 2) stacked on top of one another, with the direction of permittivity being perpendicular to the plane of the interface between the two volumes, the two volumes and the three interfaces are all in series electrically. If the contact between the two volumes is good, so that the capacitance associated with this interface is very large, then the reciprocal of this capacitance is very small and this interface contributes negligibly to the series capacitance. Under this situation,

$$1/C_m = 1/C_{i1} + 1/C_{i2} + 1/C_{v1} + 1/C_{v2}, \quad (11)$$

where C_{i1} is the interfacial capacitance of the interface between volume 1 and its electrical contact, C_{i2} is that of the interface between volume 2 and its electrical contact, and C_{v1} and C_{v2} are the volumetric capacitances of volumes 1 and 2, respectively. In case that $C_{v2} = -C_{v1}$, Eq. (11) becomes

$$1/C_m = 1/C_{i1} + 1/C_{i2}. \quad (12)$$

The case of $C_{v2} = -C_{v1}$ corresponds to

$$l_1/\kappa_1 = -l_2/\kappa_2, \quad (13)$$

where l_1 and l_2 are the thicknesses of volume 1 and volume 2, respectively, and κ_1 and κ_2 are the relative permittivity of volume 1 and volume 2, respectively. The thickness is proportional to the thickness fraction, which is proportional to the volume fraction.

Using Eq. (3), the specimen's volumetric capacitance C_v is obtained from the measured capacitance C_m, with C_i determined from the plot of $1/C_m$ versus the specimen thickness, as illustrated in Fig. 2a. The plot of $1/C_v$ versus thickness is a straight line through the origin, with the slope related to the relative dielectric constant. In order to compare different volumes in terms of the capacitance, it is important to consider C_v rather than C_m. This is because C_i, which is included in C_m, depends on the structure (e.g., the roughness) of the interface between the volume and the electrical contact. In order to obtain C_v, C_i must be known, as obtained from the intercept with the vertical axis in Fig. 2a.

A pair of negative capacitance (with negative permittivity) and positive capacitance (with positive permittivity) is chosen from the composites in Table 1, so that the magnitudes of l/κ are close. The negative capacitance chosen is the carbon fiber composite with 25-μm as-received paper (with $l/\kappa = (-1.6 \pm 0.3) \times 10^{-6}$ m, $(-2.6 \pm 0.4) \times 10^{-6}$ m, and $(-3.7 \pm 0.6) \times 10^{-6}$ m for the 3-lamina, 5-lamina, and 7-lamina composites, respectively), whereas the positive capacitance chosen is the composite with 35-μm dried paper (with $l/\kappa = (1.9 \pm 0.4) \times 10^{-6}$ m, $(3.3 \pm 0.6) \times 10^{-6}$ m, and $(4.6 \pm 0.9) \times 10^{-6}$ m for the 3-lamina, 5-lamina, and 7-lamina composites, respectively). Series connection of the negative and positive elements, each with 3 laminae, involve l/κ values that are opposite in sign but similar (not exactly equal) in magnitude ($\sim 2 \times 10^{-6}$ m). Series connection of the negative and positive elements, each with 5 laminae, involve l/κ values that are opposite in sign but similar (not exactly equal) in magnitude ($\sim 3 \times 10^{-6}$ m). Series connection of the negative and positive elements, each with 7 laminae, involve l/κ values that are opposite in sign but similar (not exactly equal) in magnitude ($\sim 4 \times 10^{-6}$ m). The two capacitances of opposite sign are stacked without bonding. Based on the linear fit to the data points for the composites with different numbers of laminae and the same sign of the permittivity (Fig. 8), each negative capacitor (irrespective of the number of laminae) is found to have $C_i = 0.145$ nF and $\kappa = -258$, and each positive capacitor (irrespective of the number of laminae) is found to have $C_i = 0.162$ nF and $\kappa = 217$.

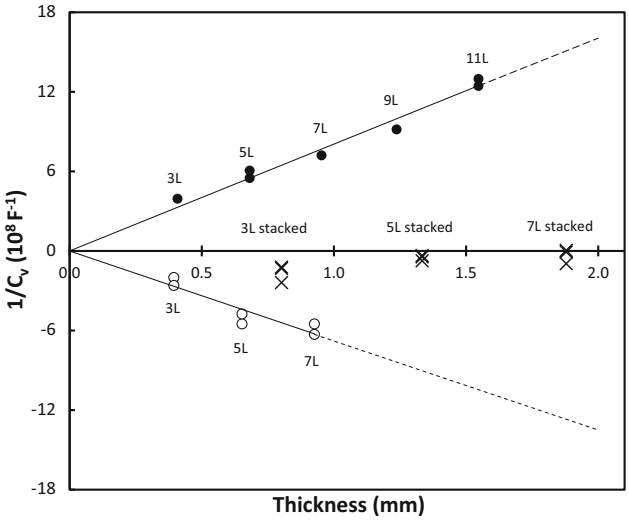

Figure 8 Plot of $1/C_v$ (1.0 MHz) versus thickness for capacitors in series and for the individual capacitors involved. The abbreviation nL refers to a composite with n laminae. For example, the abbreviation 5L refers to a stack of two 5-lamina composites with opposite signs of the permittivity; this stack has thickness corresponding to that of a 10-lamina composite. The *solid circles* are the data for an individual composite with positive permittivity (at various thicknesses), namely the carbon fiber composite with 35-μm dried paper interlayer. The *open circles* are the data for an individual composite with negative permittivity (at various thicknesses), namely the carbon fiber composite with 25-μm as-received paper interlayer. The values of the relative dielectric constant of these individual composites are shown in Table 1. The crosses are the data for the stacks of these two composites of opposite signs of the permittivity. The abbreviation "nL stacked" refers to an unbonded stack of a positive permittivity n-lamina composite and a negative permittivity n-lamina composite.

Each capacitance type tested (the different types having positive and negative signs of the capacitance) includes capacitors with different numbers of laminae. Thus, 3-lamina/5-lamina/7-lamina composites of the two types and with the same number of lamina are stacked. Figure 8 shows the results for these series combinations at 1.0 MHz. In addition, Fig. 8 shows the data for each of the capacitors involved in the series connection. As predicted by Eq. (1), the value of $1/C_v$ for the series combination is quite close to zero, while the values for the individual capacitors involved are at positive and negative values that are far from zero. Hence, the well-known equation for

capacitors in series (Eq. 1) applies to a combination of positive and negative capacitors. This finding provides a new application for negative capacitors as circuit elements for providing, along with positive capacitors, extraordinarily high permittivity.

As shown in Fig. 8, the lowest value of $1/C_v$ is given by the stack of 7-lamina composites. This lowest value is 4.23×10^6 F^{-1}, which gives $C_v = 0.24$ μF, i.e., C_v per unit area = 370 μF/m^2. The area is the geometric area of the square surface of the laminate, i.e., 6.45 cm^2. A relative dielectric constant κ of 78,000 is then obtained from the slope of the straight connecting this point and the origin of Fig. 8.

The abovementioned stacks do not involve bonding between the two composites in the stack. The use of a carbon black paste (organic-based) [52] or a graphite colloid (a dispersion of 22 wt% graphite particles of average size 0.7–0.8 mm in water, containing a starch-type binder, from Grafo Hydrograf A M2, Fuchs Lubricant Co., Emlenton, PA), as a thin interfacial medium between the two composites in the stack does not provide permittivity results that are as reproducible as the case without any interfacial medium. This is attributed to the reduced interfacial resistance provided by the interfacial medium and the importance of a sufficiently high interfacial resistance for the permittivity results.

The κ value of 78,000 is substantial compared to the highest values ever reported for any material. Values up to 180,000 were reported for polycrystalline $Ca_{1-x}Sr_xCu_3Ti_4O_{12}$ ($0 \le x \le 1$) ceramics [53]. Values up to 8400 were reported for ferroelectric $(1-x)$BZT-xBCT ceramics [53]. The materials of this paper are structural composites that can be fabricated inexpensively and provided in the form of large panels, in contrast to the high-temperature processing required for the ceramics of prior work [53, 54].

Electrical resistivity

The resistivity of the stack is obtained by measuring stacks in the form of two 3-lamina composites of opposite signs of the permittivity, two 5-lamina composites of opposite signs of the permittivity, and 7-lamina composites of opposite signs of the permittivity, and plotting the resistance versus stack thickness, as illustrated in Fig. 2b. The obtained values are 0.52 ± 0.05, 0.52 ± 0.04, 0.51 ± 0.04, and 0.51 ± 0.03 kΩ cm at 100 kHz, 500 kHz, 1.0 MHz, and 2.0 MHz, respectively. These values are between those of the individual composites in the stack (Table 1), though they are closer to the values for the negative permittivity composite than those of the corresponding positive permittivity composite.

The polarization in the negative permittivity composite is expected to promote DC conduction, whereas that in the positive permittivity composite is expected to hinder DC conduction. Under AC condition, at any instant in time, one composite (whether positive or negative in the permittivity) in the stack promotes conduction, while the other composite hinders conduction. As a consequence, the composite that has a higher resistivity would be impacted more in terms of enhanced conduction, i.e., the composite with positive permittivity will be impacted more. As a consequence, the resistivity of the stack is closer to the resistivity of the negative permittivity composite than that of the positive permittivity one.

Negligible contribution of the interlaminar interface to the dielectric or conduction behavior

If there are N laminae in a composite, there are $N-1$ interlaminar interfaces and the capacitance C_v of the specimen is given by

$$1/C_v = N\,(1/C_\ell) + (N-1)\,(1/C_f), \tag{14}$$

where C_ℓ is the capacitance of a lamina and C_f is that of an interlaminar interface. The C_ℓ and C_f may be determined by measuring C_v for different values of N.

Figure 4 shows that the plot of $1/C_m$ (where C_m is the measured capacitance) versus thickness for the composites is linear. In accordance with Eq. (14), the fact that the plot is a straight line means that

$$1/C_v = N(1/C_\ell) \tag{15}$$

$$1/C_f \approx 0. \tag{16}$$

Equation (16) means that C_f is essentially infinity, so that the interlaminar interface essentially does not contribute to the capacitance of the composite. Equation (15) means that C_ℓ is essentially the only contributor to the capacitance of the composite. In other words, the contribution by the interlaminar interfaces is negligible compared to that by the laminae. The dominance of the contribution by the laminae reflects the large number of fiber-matrix interfaces within a lamina.

A similar argument applies to the electrical resistivity. For a composite with N laminae,

$$R_v = N R_l + (N-1)R_f, \quad (17)$$

where R_v is the volume resistance of the composite, R_ℓ is the resistance of a lamina, and R_f is that of an interlaminar interface. The R_ℓ and R_f may be determined by measuring R_v for different values of N.

Figure 6 shows that the plot of R_m (the measured resistance) versus thickness for the composites is linear. In accordance with Eq. (17), the fact that the plot is a straight line means that $R_f \approx 0$, so that R_ℓ is essentially the only contributor to the through-thickness resistance of the composite. The dominance of the contribution by the laminae reflects the large number of fiber–fiber contacts within a lamina.

Conclusions

Negative permittivity, positive permittivity, and their extraordinarily high series permittivity (antiferroelectric coupling) have been achieved in continuous carbon fiber epoxy–matrix composites in the through-thickness direction, with the magnitude of the relative dielectric constant (real part, κ) up to 600, 400, and 78,000, respectively, at frequencies up to 2.0 MHz. The composite laminate tailoring involves the use of suitable dielectric interlaminar interlayers in the form of tissue paper. The composite with a paper interlayer at every interlaminar interface exhibits positive or negative values of κ, such that the magnitude is much higher than that of the corresponding paper interlayer material (with epoxy, but not as a part of the carbon fiber composite) or the corresponding standalone paper (without epoxy).

The negative and positive capacitors in series give extraordinarily high capacitance (up to 370 $\mu F/m^2$), which corresponds to κ being up to 78,000. The well-known equation for capacitors in series (Eq. 1) is found for the first time to apply to a combination of positive and negative capacitors. For the purpose of obtaining high series capacitance, positive and negative capacitors are chosen such that the magnitudes of their capacitance are close. The use of the series combination to achieve a very high permittivity has not been tried or suggested in previous work. This is the most novel part of this paper.

The κ value of 78,000 is comparable to or higher than the highest values ever reported for any material. The associated capacitance per unit geometric area of 370 $\mu F/m^2$ is much higher than the value of 1 $\mu F/m^2$ previously reported for carbon fiber composites [11]. Furthermore, the positive permittivity (κ up to 400) provided by a positive capacitor is much more positive than the most positive value (20 [11]) previously reported for carbon fiber composites.

This paper provides the first observations of negative permittivity and negative capacitance in carbon fiber composites. For materials in general, it provides the first observation of extraordinarily high permittivity resulting from the series connection of a pair of positive and negative capacitors. Moreover, this paper advances the field of structural capacitors and enables carbon fiber structural composites to be potentially attractive for environmentally friendly and large-scale electrical energy storage.

The negative permittivity requires the tissue paper to be wet with water (tap water with resistivity 1.5 kΩ cm at 1.0 MHz) during incorporation in the composite, though the water evaporates and leaves ions (at very low concentrations) and air voids during the heating in composite fabrication. In contrast to tap water, deionized water with resistivity 8 kΩ cm at 1.0 MHz gives composites with positive permittivity. The greater the wetness with tap water, the progressively more negative is the permittivity for composites with the 35-μm-thick paper. The thickness of 35 μm gives through-thickness laminate electrical resistivity (1.0 MHz) 1 kΩ cm and is optimum for obtaining negative permittivity. A thickness of 60 μm gives high resistivity 30 kΩ cm (due to a relatively small extent of fiber–fiber contact across the interlaminar interface) and positive permittivity. A thickness of 25 μm gives low resistivity 0.3 kΩ cm (due to a relatively large extent of fiber–fiber contact across the interlaminar interface) and does not give negative permittivity consistently. Without carbon fibers, the tissue paper gives positive permittivity, whether epoxy is present or not. The negative permittivity requires the presence of carbon fibers and an optimum resistivity (of the order of 1 kΩ cm). It is probably due to interactions between the functional groups on the carbon fiber surface and the residual ions (mainly chloride) left after the evaporation of water from the paper.

This work decouples the volumetric capacitance from the interfacial capacitance (at each of the two electrical contacts) by testing each material at three thicknesses. It is the volumetric capacitance rather than the measured capacitance that exhibits the effects mentioned above. Prior work did not perform

this decoupling, whether in relation to continuous carbon fiber polymer–matrix composites [11] or short carbon fiber polymer–matrix composites [55].

This work provides the first report of a negative capacitor in a material other than a ceramic ferroelectric material [56] or a ceramic antiferroelectric material [37–42]. Negative capacitors are potentially attractive for field-effect transistors with reduced voltage requirement and hence less heating [57].

Compared to the laminae, the interlaminar interfaces contribute negligibly to the dielectric or conduction behavior. Nevertheless, modification of the interlaminar interface affects the composite's dielectric and conduction behavior. This suggests that the interlayer affects the structure in a lamina, perhaps through the interaction of the ions in the interlayer with the functional groups on the carbon fibers.

Compliance with ethical standards

Conflict of interest The authors declare that they have no conflict of interest.

References

[1] Zhu J, Luo Z, Wu S, Haldolaarachchige N, Young DP, Wei S, Guo Z (2012) Magnetic graphene nanocomposites: electron conduction, giant magnetoresistance and tunable negative permittivity. J Mater Chem 22(3):835–844

[2] Gu H, Guo J, He Q, Jiang Y, Huang Y, Haldolaarachige N, Luo Z, Young DP, Wei S, Guo Z (2014) Magnetoresistive polyaniline/multi-walled carbon nanotube nanocomposites with negative permittivity. Nanoscale 6(1):181–189

[3] Kavas H, Guenay M, Baykal A, Toprak MS, Sozeri H, Aktas B (2013) Negative permittivity of polyaniline-Fe_3O_4 nanocomposite. J Inorg Organomet Polymers Mater 23(2):306–314

[4] Shi Z, Chen S, Sun K, Wang X, Fan R, Wang X (2014) Tunable radio-frequency negative permittivity in nickel-alumina "natural" meta-composites. Appl Phys Lett 104(25):252908/1–252908/5

[5] Yan K, Fan R, Shi Z, Chen M, Qian L, Wei Y, Sun K, Li J (2014) Negative permittivity behavior and magnetic performance of perovskite $La_{1-x}Sr_xMnO_3$ at high-frequency. J Mater Chem C 2:1028–1033

[6] Tsutaoka T, Fukuyama K, Kinoshita H, Kasagi T, Yamamoto S, Hatakeyama K (2013) Negative permittivity and permeability spectra of Cu/yttrium iron garnet hybrid granular composite materials in the microwave frequency range. Appl Phys Lett 103(26):261906/1–261906/5

[7] Wang D, Chung DDL (2013) Through-thickness piezoresistivity in a carbon fiber polymer-matrix structural composite for electrical-resistance-based through-thickness strain sensing. Carbon 60(1):129–138

[8] Chung DDL (2007) Damage detection using self-sensing concepts. J Aerospace Eng (Proceedings of the Institution of Mechanical Engineers, Part G) 221(G4):509–520

[9] Han S, Chung DDL (2013) Through-thickness thermoelectric power of a carbon fiber/epoxy composite and decoupled contributions from a lamina and an interlaminar interface. Carbon 52:30–39

[10] Han S, Chung DDL (2013) Carbon fiber polymer-matrix structural composites exhibiting greatly enhanced through-thickness thermoelectric figure of merit. Compos A 48:162–170

[11] Luo X, Chung DDL (2001) Carbon fiber polymer-matrix composites as capacitors. Compos Sci Tech 61:885–888

[12] Tony T, Asp LE (2013) Structural carbon fibre composite/PET capacitors—effects of dielectric separator thickness. Compos B 49:16–21

[13] Carlson T, Ordeus D, Wysocki M, Asp LE (2010) Structural capacitor materials made from carbon fibre epoxy composites. Compos Sci Technol 70(7):1135–1140

[14] Jiang Q, Yang R, Fu GG, Xie DY, Huang B, He ZW, Zhao Y (2011) Preparation of the carbon nanotube/carbon fiber composite and application as the electrode material of the electrochemical super capacitor. Mater Sci Forum 687:158–162

[15] Salinas-Torres D, Sieben JM, Lozano-Castello D, Cazorla-Amoros D, Morallon E (2013) Asymmetric hybrid capacitors based on activated carbon and activated carbon fibre-PANI electrodes. Electrochim Acta 89:326–333

[16] Jin Z, Tian Y, Su LJ, Qin CL, Zhao DY, Li RQ, Zhao J (2013) Hybrid supercapacitors based on polyaniline/activated carbon fiber composite electrode materials. In: Advanced Materials Research (Durnten-Zurich, Switzerland) vol. 800, pp. 505–508

[17] Asp LE (2013) Multifunctional composite materials for energy storage in structural load paths. Plast, Rubber Compos 42:144–149

[18] Leijonmarck S, Carlson T, Lindbergh G, Asp LE, Maples H, Bismarck A (2013) Solid polymer electrolyte-coated carbon fibres for structural and novel micro batteries. Compos Sci Technol 89:149–157

[19] Jacques E, Kjell MH, Zenkert D, Lindbergh G, Behm M, Willgert M (2012) Impact of electrochemical cycling on the tensile properties of carbon fibres for structural lithium-ion composite batteries. Compos Sci Technol 72:792–798

[20] Pereira T, Guo Z, Nieh S, Arias J, Hahn HT (2009) Energy storage structural composites: a review. J Compos Mater 43:549–560

[21] Han S, Chung DDL (2011) Increasing the through-thickness thermal conductivity of carbon fiber polymer-matrix composite by curing pressure increase and filler incorporation. Compos Sci Technol 71:1944–1952

[22] Chung DDL (2004) Self-heating structural materials. Smart Mater Struct 13(3):562–565

[23] Han S, Chung DDL (2012) Mechanical energy dissipation using carbon fiber polymer-matrix structural composites with filler incorporation. J Mater Sci 47:2434–2453. doi:10.1007/s10853-011-6066-7

[24] Luo X, Chung DDL (1999) Electromagnetic interference shielding using continuous carbon fiber carbon-matrix and polymer-matrix composites. Compos B 30:227–231

[25] Chung DDL (2001) Electromagnetic interference shielding effectiveness of carbon materials. Carbon 39:279–285

[26] Wu J, Chung DDL (2002) Increasing the electromagnetic interference shielding effectiveness of carbon fiber polymer-matrix composite by using activated carbon fibers. Carbon 40(ER3):445–447

[27] Chung DDL (2012) Carbon materials for structural self-sensing, electromagnetic shielding and thermal interfacing. Carbon 50:3342–3353

[28] Wang R, Yang H, Wang J, Ma Z, Li F (2014) Preparation and characterization of conductive filler used for electromagnetic shielding materials. Appl Mech Mater 492:268–272

[29] Liu L, He P, Zhou K, Chen T (2014) Microwave absorption properties of carbon fibers with carbon coils of different morphologies (double microcoils and single nanocoils) grown on them. J Mater Sci 49(12):4379–4386. doi:10.1007/s10853-014-8137-z

[30] Yuan Q, Su C, Huang J, Gan W, Huang Y (2013) Process and analysis of electromagnetic shielding in composite fiberboard laminated with electroless nickel-plated carbon fiber. BioResources 8:4633–4646

[31] Singh BP, Choudhary Saini VP, Mathur RB (2012) Designing of epoxy composites reinforced with carbon nanotubes grown carbon fiber fabric for improved electromagnetic interference shielding. AIP Adv 2:022151

[32] Singh AP, Garg P, Alam F, Singh K, Mathur RB, Tandon RP, Chandra A, Dhawan SK (2012) Phenolic resin-based composite sheets filled with mixtures of reduced graphene oxide, γ-Fe_2O_3 and carbon fibers for excellent electromagnetic interference shielding in the X-band. Carbon 50:3868–3875

[33] Wang R, He F, Wan Y, Qi Y (2012) Preparation and characterization of a kind of magnetic carbon fibers used as electromagnetic shielding materials. J Alloys Compd 514:35–39

[34] Mall S, Rodriguez J, Alexander MD (2011) Electromagnetic interference and electrical conductivity behavior of carbon/polycyanate composite with nickel nanostrands™ under fatigue. Polym Compos 32:483–490

[35] Hua Y, Yamanaka A, Ni Q (2010) Electromagnetic shielding properties of super fiber-reinforced composites. Adv Mater Res (Zurich, Switzerland) 123–125:65–68

[36] Micheli D, Laurenzi S, Mariani PV, Moglie F, Gradoni G, Marchetti M (2012) Electromagnetic Shielding of Oriented Carbon Fiber Composite Materials. European Space Agency [Special Publication] SP-702:a3/1

[37] Belov DA, Shlyakhtina AV, Stefanovich SY, Shchegolikhin AN, Knotko AV, Karyagina OK, Shcherbakova LG (2011) Antiferroelectric phase transition in pyrochlore-like $(Dy_{1-x}Ca_x)_2Ti_2O_{7-\delta}$ ($x = 0, 0.1$) high temperature conductors. Solid State Ionics 192(1):188–194

[38] Korotkov L, Likhovaya D, Levitskii R, Sorokov S, Vdovych A (2013) Dielectric, elastic and electromechanical properties of $K_{1-x}(NH_4)_xH_2PO_4$ solid solutions in paraelectric phase. Ferroelectrics 444(1):76–83

[39] Yasuda N, Kawai J (1990) Dielectric dispersion associated with the d.c.-electric-field-enforced ferroelectric phase transition in the pressure-induced antiferroelectric cesium dihydrogen phosphate. Phys Rev B: Condens Matter 42(7-B):4893–4896

[40] Tang H, Feng YJ, Xu Z, Zhang CH, Gao JQ (2009) Effect of Nb doping on microstructure and electric properties of lead zirconate stannum titanate antiferroelectric ceramics. J Mater Res 24(5):1642–1645

[41] Zhang Q, Chen S, Fan M, Jiang S, Yang T, Wang J, Li G, Yao X (2012) High pyroelectric response of lead zirconate stannate titanate based antiferroelectric ceramics with low Curie temperature. Mater Res Bull 47(12):4503–4509

[42] Zhuo F, Li Q, Li Y, Gao J, Yan Q, Zhang Y, Chu X, Cao W (2014) Effect of A-site La^{3+} modified on dielectric and energy storage properties in lead zirconate stannate titanate ceramics. Mater Res Express 1(4):045501/045501–045501/045511

[43] Grimberg R (2013) Electromagnetic metamaterials. Mater Sci Eng B 178(19):1285–1295

[44] Chawla KK (2005) Fibrous materials. Cambridge University Press, Cambridge, p 55

[45] Wang A, Chung DDL (2014) Dielectric and electrical conduction behavior of carbon paste electrochemical electrodes, with decoupling of carbon, electrolyte and interface contributions. Carbon 72:135–151

[46] Hong X, Chung DDL (2015) Exfoliated graphite with relative dielectric constant reaching 360, obtained by exfoliation of acid-intercalated graphite flakes without subsequent removal of the residual acidity. Carbon 91:1–10

[47] Moalleminejad M, Chung DDL (2015) Dielectric constant and electrical conductivity of carbon black as an electrically

conductive additive in a manganese-dioxide electrochemical electrode, and their dependence on electrolyte permeation. Carbon 91:76–87

[48] Dhakate SR, Bahl OP (2003) Effect of carbon fiber surface functional groups on the mechanical properties of carbon–carbon composites with HTT. Carbon 41:1193–1203

[49] Fukai K, Hidaka K, Aoki M, Abe K (1990) Preparation and properties of uniform fine perovskite powders by hydrothermal synthesis. Ceram Int 16:285–290

[50] Wang S, Chung DDL (2005) The interlaminar interface of a carbon fiber epoxy-matrix composite as an impact sensor. J Mater Sci 40:1863–1867. doi:10.1007/s10853-005-1205-7

[51] Wang S, Kowalik DP, Chung DDL (2004) Self-sensing attained in carbon fiber polymer-matrix structural composites by using the interlaminar interface as a sensor. Smart Mater Struct 13:570–592

[52] Leong C, Aoyagi Y, Chung DDL (2005) Carbon-black thixotropic thermal pastes for improving thermal contacts. J Electron Mater 34(10):1336–1341

[53] Lee SY, Yoo D, Lee J, Jo W, Hong Y, Kim Y, Yoo S (2012) Fabrication and characterization of colossal dielectric response of polycrystalline $Ca_{1-x}Sr_xCu_3Ti_4O_{12}$ ($0 \leq x \leq 1$) ceramics. MRS Online Proceedings Library, Vol. 1454, Nanocomposites, Nanostructures and Heterostructures of Correlated Oxide Systems

[54] Puli VS, Pradhan DK, Chrisey DB, Tomozawa M, Sharma GL, Scott JF, Katiyar RS (2013) Structure, dielectric, ferroelectric, and energy density properties of (1 − x)BZT–xBCT ceramic capacitors for energy storage applications. J Mater Sci 48:2151–2157. doi:10.1007/s10853-012-6990-1

[55] Dang Z, Zhang Y, Tjong S (2004) Dependence of dielectric behavior on the physical property of fillers in the polymer-matrix composites. Synth Met 146(1):79–84

[56] Khan AI, Chatterjee K, Wang B, Drapcho S, You L, Serrao C, Bakaul SR, Ramesh R, Salahuddin S (2015) Negative capacitance in a ferroelectric capacitor. Nat Mater 14:182–186

[57] Catalan G, Jimenez D, Gruverman A (2015) Ferroelectrics negative capacitance detected. Nat Mater 14(2):137–139